European Journal of Neuroscience, Vol. 5, pp. 437–448

Current Source Density Profiles of Optical Recording Maps: a New Approach to the Analysis of Spatio-temporal Neural Activity Patterns

Dietmar Plenz[1] and Ad Aertsen[1,2]
[1]Max-Planck-Institut für biologische Kybernetik, Spemannstrasse 38, D-7400 Tübingen, Germany
[2]Institut für Neuroinformatik, Ruhr-Universität, PO Box 102148, D-4630 Bochum, Germany

Key words: current source density analysis, optical recording, voltage-sensitive fluorescent dyes, rat, hippocampal slice, CA1

Abstract

Spatio-temporal spreading of activity in the CA1 region of the rat hippocampal slice was studied by two experimental approaches. At identical locations in the tissue we measured both the extracellular field potential distribution with microelectrode recordings and the intracellular potential distribution by optical recording, using voltage-sensitive fluorescent dyes. Current source density analysis (CSD) was applied to the extracellular field potential distributions (eCSD) to enhance the spatial resolution. In order to obtain an analogous improvement for the optical recordings, we developed a new CSD transformation, which calculates the locations of the transmembrane current generators from the intracellular potential distributions (iCSD). Compared to the underlying fluorescence maps, the new iCSD profiles exhibit a considerable improvement in spatial resolution. Results can be directly interpreted in terms of physiological membrane processes, such as postsynaptic potentials and action potentials. The iCSD profiles show a surprisingly good correspondence with the classical eCSD profiles both qualitatively and quantitatively, the only difference being that cell body activity is reduced in amplitude. Thus, this new optical CSD analysis paves the way for a quantitative interpretation, rather than the hitherto predominantly qualitative interpretation of spatio-temporal activity profiles from optical recording measurements.

Introduction

Functional interactions within and between neuronal populations can be assessed by measuring the spatio-temporal spreading of nervous activity. In principle, this can be accomplished in two different ways: by examination of the voltage distribution in extracellular space or, alternatively, by intracellular measurement of the activity of the cells involved. For a long time, the only feasible approach was to measure the extracellular field potential distribution as a function of time. This method, however, suffered from an inadequate spatial resolution, due to the superposition of potentials induced by large numbers of spatially distributed current generators: synaptic events and currents due to voltage-gated channel activity. This spatial resolution could only be significantly enhanced after the studies of Nicholson and Freeman (1975), who introduced the interpretation of neuronal activity at the level of transmembrane current densities, following the pioneering work of Pitts, McCulloch and colleagues (Pitts, 1952; Howland *et al.*, 1955). In particular, they showed that with a specifically designed current source density (CSD) analysis of the field potential distribution, it is possible to measure the spatial distribution of the transmembrane current generators. Thereby, they attained a spatial resolution of down to 20 μm, while retaining the (sub)millisecond time resolution provided by the normal electrophysiological setup. This development led to a considerable body of experimental work, in which CSD analysis was applied to a variety of different brain areas (for a review see Mitzdorf, 1985). In order to avoid a number of practical problems associated with multiple-microelectrode recordings, a considerable portion of the CSD literature restricts this analysis to a one-dimensional problem, whenever this was allowed by the anatomy of the tissue under study and the stimulus and recording arrangement. In the present contribution we will adopt this approach as well.

Recently, another technique was introduced to map the spatio-temporal dynamics of neural activity over an extended area of nervous tissue. This new technique of 'optical recording' consists of measuring the changes in optical properties of the tissue brought about by neural activity (Cohen *et al.*, 1968; Tasaki *et al.*, 1969; Cohen and Salzberg, 1978; Grinvald *et al.*, 1988; Salzberg, 1989). Such changes can be determined directly from the intrinsic properties of the tissue itself or, indirectly, by applying activity-dependent dyes to the cell membranes. An important example of the latter are the voltage-sensitive fluorescent dyes, which change the amplitude of their fluorescence signal in proportion to the local voltage gradient between the intra- and extracellular space (Waggoner, 1979; Grinvald *et al.*, 1982a). The latency and amplitude distributions of these optical signals, however, fail to achieve the spatial resolution obtained with CSD analysis. This is not only due to the problem of determining the actual source(s) of the optical signals (e.g.

Correspondence to: Dietmar Plenz, as above

Received 27 November 1991, revised 24 November 1992, accepted 18 December 1992

nerve cells or glia cells; Lev-Ram and Grinvald, 1986; Konnerth *et al.*, 1987), but also to the spreading of intracellular potentials by conduction of the various nerve cell elements. In this respect, the optical signals, which can be regarded as reflecting the 'intracellular population activity' (Grinvald, personal communication), suffer from very much the same problem as the field potential measurements of the 'extracellular population activity'. In addition, and partly related to this, the interpretation of spatio-temporal activity patterns revealed in optical recordings has until now been predominantly qualitative rather than quantitative, due to the lack of an appropriately calibrated scale of reference.

Inspired by these common features of intra- and extracellular potential distributions, we developed a CSD transformation for optical recording signals. This new approach adopts the differentiating and hence 'contrast-enhancing' operation of classical CSD analysis. Thus, it enables us to calculate the locations of the transmembrane current generators from the fluorescence maps. We rigorously identified the fluorescence signals with the intracellular population activity, integrated over a number of nerve cells or nerve cell circuits per unit tissue volume, and calculated from these signals the transmembrane current densities as viewed from the intracellular space. In view of the many intricate problems of cell geometry, resistances in intra- and extracellular space, signal sources, differential binding of the various dyes (e.g. Orbach *et al.*, 1985) and the like, it is evident that the question of whether it is possible to calculate a meaningful CSD profile for a particular nerve tissue preparation on the basis of fluorescence signals can ultimately be resolved only on the basis of a direct physiological test. A crucial issue in this respect is to what extent a qualitative, and preferably quantitative, agreement can be obtained between the electrophysiological and optophysiological CSD profiles. We addressed this issue by measuring both the extracellular field potential distribution and the fluorescence distribution at the same locations in a nervous tissue preparation. Recordings were made from the CA1 region of the rat hippocampal slice; by virtue of its orderly topography, this preparation allows a reduction of the CSD analysis to one dimension only. CSD profiles were then computed from both sets of measurements, and the resulting patterns compared for (dis)similarities. A preliminary description of this new approach to the analysis of optical recording signals has appeared in abstract form (Plenz and Aertsen, 1991).

Materials and methods

Slice preparation

For the preparation of hippocampal slices, adult rats (Lewis) aged 4–6 weeks were anaesthetized with ketamine (150 mg/kg i.p.) and decapitated. The brains were quickly removed and cooled in a solution of artificial cerebrospinal fluid (ACSF) at 4°C (124 mM NaCl, 1.25 mM KH_2PO_4, 5 mM KCl, 3.6 mM $CaCl_2$, 1.3 mM $MgSO_4$, 26 mM $NaHCO_3$, 9.4 mM D-glucose). For the first part of the preparation 25 mg ketamine/100 ml ACSF solution was added (ACSFKet). Transverse hippocampal slices were cut with an 'egg slicer' (400 μm thick; Katz, 1987) or on a vibratome (300 μm). Slices were stored at 33.0±0.1°C on thin pieces of membrane filter (Nucleopor, 12 μm), submerged in ACSFKet saturated with carbogen (95% O_2/5% CO_2). The flow rate in the storage chamber was set to 1 ml/min. After 30 min the ACSFKet solution was exchanged for pure ACSF. In order to minimize signal contributions from cells that were injured in the preparation procedure, slices were kept in the storage chamber for a long recovery period (5–6 h) before the first recordings were made.

For recording, a slice was transferred to the recording chamber, which was mounted on an inverted microscope (Zeiss, IM35), equipped with an epifluorescence filter set (Zeiss, BP 546, FT 580, LP 590). The chamber was continuously perfused with ACSF at a flow rate of 0.5 ml/min; specific care was taken to maintain the entire preparation at a highly constant temperature (33.0±0.1°C). The slice was lying submerged on a thin glass coverslip. Thus, optical recordings could be made from below, while the space above the chamber was available for electrophysiological manipulations. The voltage-sensitive styryl dye RH237 was applied to the bathing medium before the experiment, after which perfusion was stopped for 15 min. After recommencing perfusion, the experiment was started once the extracellular field potential became stable for at least 30 min. Monopolar tungsten microelectrodes were used for electrical stimulation of the Schaffer collaterals and the alveus. Single or double pulses (duration 50 μs, interpulse interval 30 ms) with a constant amplitude between 150 and 500 μA were applied at a frequency of 0.2 Hz.

Electrophysiology

Extracellular field potentials were recorded with a glass micropipette filled with 3 M NaCl (6–12 MΩ impedance). Recordings were made at a constant depth between 70 and 100 μm below the surface of the slice, using an electrically controlled micromanipulator (Piezo manipulator PM10, Merzhäuser). Successive recording positions, separated by either 30 or 60 μm, were situated along a linear path, orientated orthogonally to the CA1 pyramidal cell layer (Fig. 1c: Rec., Electrode Path). The adequacy of this spatial resolution was checked by spatial Fourier analysis of the field potential distributions (Plenz and Aertsen, 1993). At each recording site, ten consecutive responses were recorded and used for later averaging. In order to obtain large responses, long-term potentiation was induced ~30 min before starting field potential measurements by delivering 4–6 stimulus trains (30 pulses at 50 Hz, interstimulus interval 5 s) to the Schaffer collaterals. The stability of the recording was checked by measuring the field potential at one location in the CA1 region with a second electrode throughout the entire experiment (Fig. 1c: Cont.). In addition, we checked the activity of the tissue at different locations along the electrode path after the field potential distribution was obtained.

Electrical signals were recorded with a conventional electrophysiological setup, bandpass filtered between 1 Hz and 1 kHz, digitized at a rate of 3.3 kHz, and stored in a microcomputer (DEC LSI 11/73), from which the data were transferred to a Vax 750 (DEC) for further processing. From the sets of 23–35 field potentials per electrode path (each being the result of averaging over ten trials) we computed one-dimensional CSD profiles according to the method described by Mitzdorf (1985). We assumed that (1) the electric field is quasi-static, and (2) the extracellular space has the properties of an ohmic conductor with approximately constant conductivity in the direction of the electrode path (Holsheimer, 1987). Under these assumptions the CSD profile is proportional to the second-order spatial derivative of the field potential distribution. Moreover, since the field potentials change only slightly when progressing along the CA1 layer as compared to the profound changes measured in the direction perpendicular to it (Novak and Wheeler, 1989), the true CSD distribution can be approximated by applying one-dimensional CSD analysis (Mitzdorf, 1985) according to the formula:

$$-I_m(z,t) \sim \frac{U(z - n\Delta h,t) - 2U(z,t) + U(z + n\Delta h,t)}{(n\Delta h)^2} \quad (1)$$

where $I_m(z,t)$ indicates the transmembrane current density at position z and time t, $U(z,t)$ is the field potential distribution, Δh denotes the sampling interval between adjacent recording locations, and $n\Delta h$ is the differentiation grid size. In the CSD profiles shown, the sampling interval

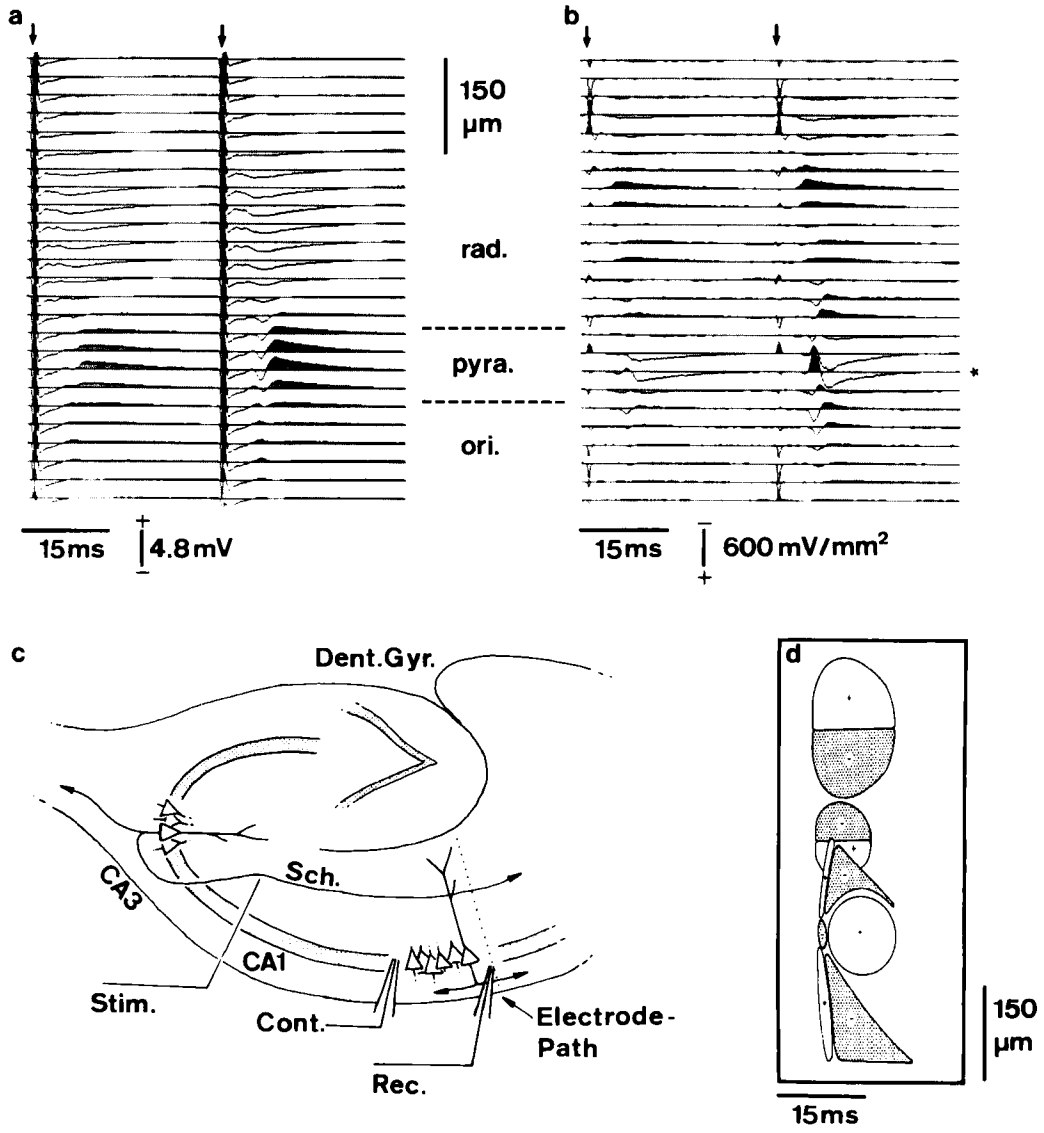

FIG 1. Example of a CSD profile in the CA1 region of the rat hippocampal slice, in response to double-pulse stimulation of the Schaffer collaterals. Stimulus pulses are indicated by arrows along the time axes (top). (a) Field potential distribution, with positive deflections drawn upwards. (b) CSD profile, with sinks drawn upwards and sources downwards. (c) Sketch of the recording situation. (d) Schematic outline of sink and source profiles in (b), with sink profiles filled with a dot raster. In this and in all subsequent figures, polarity in the various distributions is indicated by the + and − signs on the vertical scale bars. Dent.Gyr., gyrus dentatus; Sch., Schaffer collaterals; rad., stratum radiatum; pyra., stratum pyramidale; ori., stratum oriens; Stim., stimulus electrode; Cont., control electrode; Rec., recording electrode; Electrode Path, sketch of successive recording electrode positions.

was either 30 μm with $n = 2$ (Fig. 1) or 60 μm with $n = 1$ (all other Figs).

Optophysiology

For optical recording, the slice was illuminated by a mercury lamp (Zeiss, HWO 100 W/2) with a stabilized power supply (Siemens). The image of the slice, focused at a depth of 200–300 μm below the slice surface, was projected with an objective (Leitz, 25× NPL Fluotar, 0.75 oil-immersion) onto a 12×12 photodiode array (Centronics, M144–5). Voltage-dependent fluorescent dye signals from 128 of these photodiodes, covering a circular field of view, were amplified, multiplexed and fed into a microcomputer (DEC LSI 11/73) at a sampling rate of 2 kHz per channel. After the experiment, the data were transferred to a VAX 750 (DEC) for further processing. In order to minimize photodynamic damage to the tissue (Ross *et al.*, 1977), trials were kept short (duration of illumination 96 ms), the number of stimuli for averaging was restricted to six per field, and trials were separated by long recovery intervals (30 s; Bonhoeffer and Staiger, 1988). We ascertained stationarity of the recording by additionally monitoring tissue activity with an extracellular microelectrode throughout the optical measurements.

In order to correct for bleaching, the fluorescence change dF for each time step was calculated for separate locations as the difference in fluorescence between successive trials with and without a stimulus or, alternatively, as the difference between the response to a stimulus and a linearly descending ramp. The relative fluorescence change dF/F was obtained by dividing the difference dF by the absolute fluorescence at the same location (Grinvald *et al.*, 1988). This procedure corrects to a first approximation for spatial inhomogeneities in illumination and dye distribution (for a detailed description of the optical recording setup and associated signal processing see Bonhoeffer and Staiger, 1988). Each

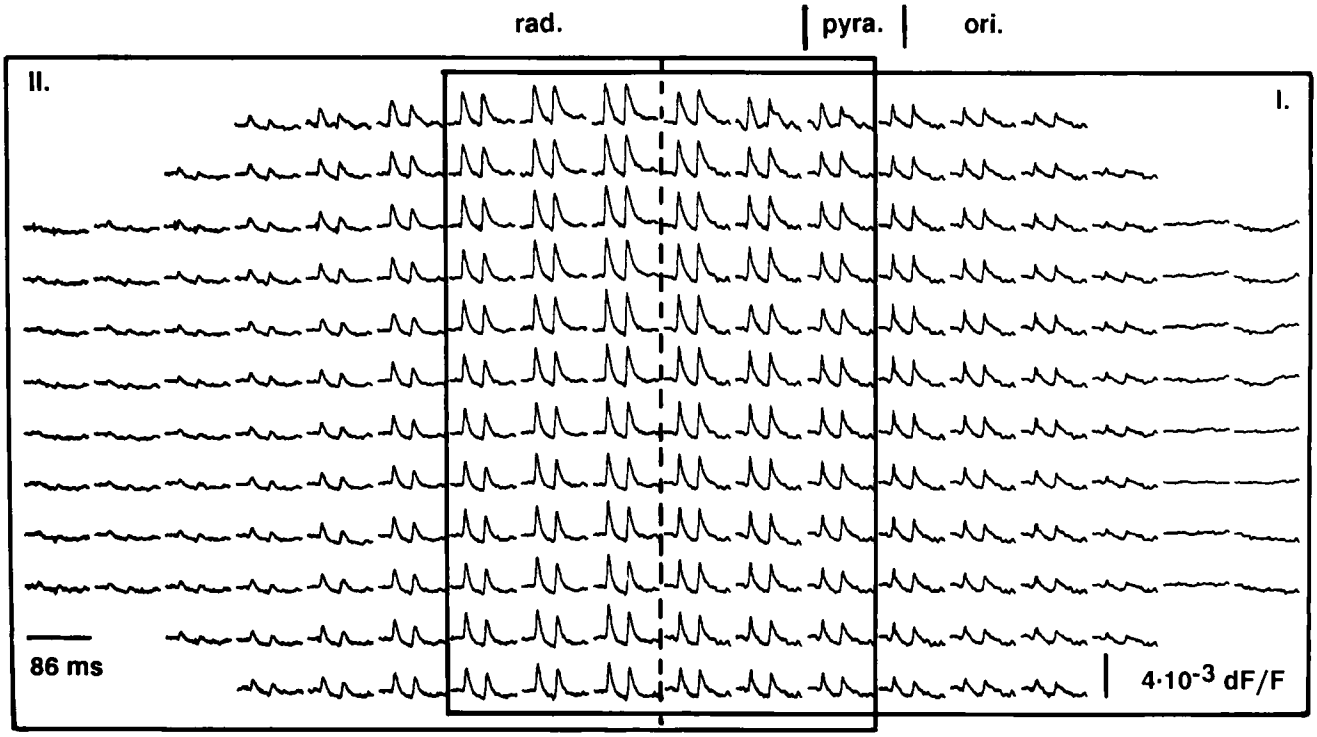

FIG. 2. Optical recording of activity in the CA1 region of the rat hippocampal slice evoked by double-pulse stimulation of the Schaffer collaterals. The tissue was stained with the voltage-dependent fluorescent dye RH237. Each trace displays the averaged activity (six stimuli) recorded by the photodiode from the corresponding location in the tissue (spatial resolution 60 μm). In order to cover the entire depth of the CA1 region, two 12×12 photodiode fields (frames I and II) were measured separately, cut (as indicated by the broken line) and merged, resulting in an array of 18×12 measurement sites. Anatomical borders are indicated on top. Upward deflection indicates intracellular depolarization.

photodiode integrated the fluorescence over an area of 60×60 μm^2. In order to cover the entire depth of the CA1 region at this high resolution, in some cases we made a montage of two partially (50%) overlapping 12×12 fields. These two (frames 1 and 2) were recorded during one experiment (12 trials) by shifting the microscope back and forth with respect to the recording chamber between trials, according to the repeated frame sequence $1-2-2-1-1-2$. The two 12×12 fields, averaged over the six corresponding trials, were merged, thus simulating an 18×12 photodiode array (Fig. 2).

In order to bring the optical and electrical recordings into register, the two coordinate systems (photodiode array and micromanipulator with electrode tip) were calibrated outside the slice at the bottom of the recording chamber and extrapolated linearly onto the slice surface. From the photodiode matrix we then selected the one-dimensional array of photodiodes which matched the recording positions of the extracellular recordings (within an accuracy of 30 μm) and used this array for the calculation of fluorescence-based CSD profiles.

Results

In 17 hippocampal slice experiments, we recorded using both electrophysiological and optophysiological methods, and were able to match the locations of the extracellular and fluorescence recordings. For the resulting pairs of activity maps (ten with stimulation of the Schaffer collaterals, seven with alveus/stratum oriens stimulation), we compared the latency and amplitude distributions as well as the associated CSD profiles. In order to distinguish between the two types of profiles, we will refer to them as 'eCSD' (based on the extracellular field potential distribution) and 'iCSD' (based on the intracellular potential distribution).

Field potential distributions and eCSD profiles

A typical example of the response in the CA1 region to orthodromic stimulation is shown in Figure 1: the field potential distribution in response to double-pulse stimulation of the Schaffer collaterals is shown in Figure 1a and the corresponding eCSD profile in Figure 1b. The lower traces originate from the outer region of CA1, the upper traces from the distal dendritic region. In the upper half of Figure 1b (stratum radiatum), both responses show a prominent pattern of a sink and an adjacent source above it, and a similar but less pronounced pattern somewhat below it. The lower half of Figure 1b (stratum oriens, stratum pyramidale and the proximal part of stratum radiatum) is considerably more complex. At the location marked with a star we observe, particularly clearly in the second response, a central sink with adjacent sources above and below it, immediately followed by an approximately inverse distribution of a prominent source with adjacent sinks. In order to facilitate the recognition of these sink/source configurations, their boundaries are redrawn schematically for the second response in Figure 1d. Notice that the two early sources in the lower part of the second response are very narrow in time and have an increasing delay with increasing distance from the central sink.

Inspection of the CSD profile, taking into account the (dis)similarities between the first and the second, facilitated response, leads us to the following interpretation. The two dipole-like sink/source distributions in the stratum radiatum represent spatially separated, synaptic inputs from the Schaffer collaterals. The sink is caused by an influx of sodium and/or calcium (Benardo *et al.*, 1982), compensated for by passive sources in the neighbouring dendritic region. The eCSD profile in the lower half of the picture reflects the highly synchronized action potentials generated in the stratum pyramidale and leading to a clear population spike

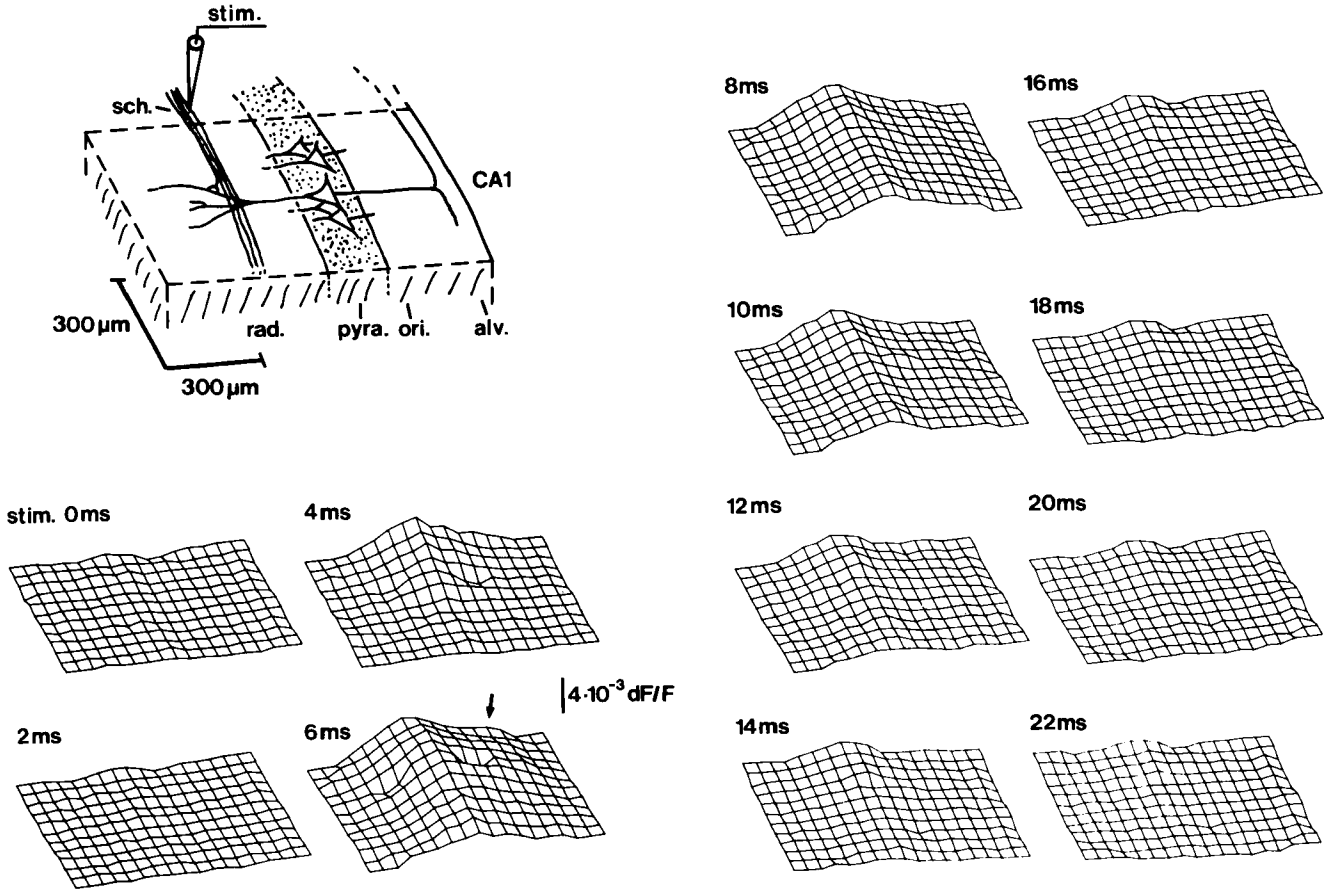

FIG. 3. Temporal development of the relative fluorescence distribution for the response to the first stimulus pulse in Figure 2. Each node in a frame displays the averaged activity (six stimuli) recorded by a photodiode from the corresponding location of the tissue at a particular instant in time; subsequent frames correspond to consecutive time steps (taken at 2-ms intervals), with the delay to the stimulus indicated at the upper left of each frame. The corners of the raster where no fluorescence was measured (outside the microscope's field of view) were set to zero for comparison. Upward deflection indicates intracellular depolarization. The stimulus arrangement and the location of the photodiode array in the CA1 region are indicated at the upper left. pyra., stratum pyramidale; ori., stratum oriens; rad., stratum radiatum; alv., alveus; stim., stimulus electrode; sch., Schaffer collaterals.

(Andersen *et al.*, 1971) in the second, enhanced response. The primary sink (indicated by the star), slightly delayed with respect to the sinks in the upper part of the stratum radiatum, is again due to positive ion influx (sodium, calcium), compensated for by passive sources in the axonal and proximal dendritic regions. The ensuing source is generated by potassium efflux, again with compensations from adjacent locations. Thus, at the site of generation (star), the action potential pattern in the eCSD profile is characterized by a typical biphasic sink/source profile. The propagation of action potentials is a further influence that shapes the spatio-temporal characteristics of the action potential pattern. Action potentials, generated in the stratum pyramidale, propagate into the basal dendrites and axons in the stratum oriens (Richardson *et al.*, 1987) and back into the stratum radiatum, thereby becoming increasingly scattered in space and time. This is reflected in the dovetail-like shapes outlined in the lower half of Figure 1d. Thus, the phenomenon of double-pulse facilitation (Creager *et al.*, 1980), with its selective enhancement of the second response, enabled us to separate the CSD patterns generated by passive synaptic events from those that involve additional active processes.

Amplitude and latency distributions of optical recording maps

In the preceding section, we demonstrated the spatio-temporal separation of active and passive processes in different strata of the CA1 region, even though only one dimension was considered. In order to evaluate to what extent such results can also be obtained from the amplitude and latency distributions in an array of optical signals, we present a typical example of such an activity map in two commonly used types of display.

Figure 2 shows, in a highly compressed way, the entire 18×12 matrix of responses to double-pulse stimulation of the Schaffer collaterals. Although this picture contains all the available information, a better impression is obtained by presenting the time course of the activity in a series of three-dimensional amplitude plots, as given in Figure 3. Each of these plots shows the spatial distribution of relative fluorescence change at a particular instant in time, with a positive deflection signifying depolarization; successive frames correspond to consecutive time steps at 2-ms intervals. No significant depolarizations are observed at stimulus onset. After 4 ms a first wave of depolarization appears in the stratum radiatum, after 6 ms a less pronounced depolarization (arrow in Fig. 3) appears at the stratum pyramidale/stratum oriens border. As time proceeds, these depolarizations slowly decay. We propose that the first change in relative fluorescence reflects synaptic potentials, generated by the Schaffer collateral input, whereas the second one is due to action potentials elicited in the stratum pyramidale.

These observations on the spatio-temporal distribution of relative fluorescence change are in accordance with general expectations based on the anatomical structure and the stimulus conditions. When compared

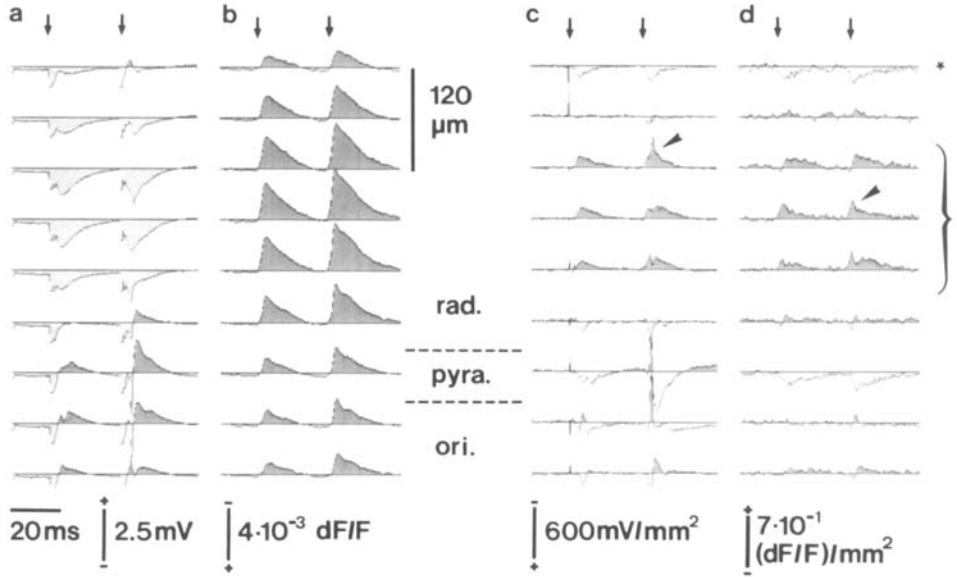

FIG. 4. Correspondence of the eCSD profile, calculated on the basis of extracellular field potential distribution, and the iCSD profile, calculated on the basis of the relative fluorescence change distribution. Response to double-pulse stimulation of the Schaffer collaterals. (a) Field potential distribution. (b) Distribution of relative fluorescence change. (c) eCSD profile; sinks are drawn upwards, sources downwards; (d) iCSD profile; sources are drawn upwards, sinks downwards. Stimulus pulses are indicated by arrows along the time axes (top). Observe that the synaptic sink (bracket) and its adjacent source in the more distal dendritic region (★) are at the same locations in both CSD profiles. Both sink profiles exhibit a spatially extended, slow component (passive synaptic events) and spatially restricted, fast components (arrowheads), the latter possibly related to 'hot spots'. Notice that the iCSD also reveals the generation and propagation of action potentials in the stratum pyramidale (lower four traces in d), albeit at distinctly lower amplitude than in the eCSD profile (c), particularly in the stratum pyramidale. Further details as in Figure 1.

to the one-dimensional CSD profiles (Fig. 1), however, the fluorescence maps show surprisingly few details. Also, the only other study on optical recording maps of area CA1 in the hippocampal slice (Grinvald *et al.*, 1982b), in spite of its somewhat better spatial resolution (45 compared to 60 μm), does not provide significantly more details than can be gathered from Figures 2 and 3. In view of these findings, we are forced to conclude that the results of straightforward visual inspection of the fluorescence distributions, even for a two-dimensional matrix of measurement sites, are rather disappointing.

CSD analysis of optical recording maps: iCSD profiles

The observed shortcomings of the fluorescence maps in providing spatial detail reflect the combined result of two sources of dispersion, which are inherent in the very nature of the optical signals. First, each physiological electrical event, even at a locally restricted patch of membrane, is dispersed by the effect of voltage propagation, due to the passive or active membrane properties at that particular site and its immediate surroundings. This effect of voltage spreading will cause a point event to show up in successive time steps in the fluorescence over a sizeable neighbourhood surrounding its site of origin. In addition to this propagation effect, comparable to a 'point spread function', each single photodiode integrates the fluorescence contributions over a certain area of tissue (including contributions by out-of-focus signals and light scattering by the tissue), the extent of which is determined by the diode's field of view. The result is a superposition of many elementary events, all slightly scattered in space and time, which reduces the spatial resolution even further. In these two respects, the fluorescence distribution is quite comparable to the extracellular field potential distribution: this also shows a considerable loss of spatial detail, due to similar effects of voltage spreading and spatial integration by the microelectrode's field of view. For the field potential distribution, the effects of voltage spreading could be overcome by the differentiating operations inherent in CSD analysis (Equation 1). Inspired by this analogy and with the same goal in mind, we set out to calculate the locations of the transmembrane current generators from the fluorescence maps, in much the same way as is done in regular CSD analysis of extracellular field potential distributions.

Figure 4 shows the results of electro- and optophysiological measurements made in the same preparation. The field potential distribution in response to double-pulse stimulation of the Schaffer collaterals (Fig. 4a) shows a population spike in the stratum pyramidale, which is small in the first, but fully developed in the second, facilitated response. The same holds for the associated eCSD profile (Fig. 4c): one observes, faintly in the first, but distinctly in the second response, the typical sink/source distribution of action potentials, generated in the stratum pyramidale and propagated into the stratum oriens. In addition, a distinct synaptic sink is observed in the middle region of the stratum radiatum, with adjacent sources in the distal dendritic region and towards the cell body layer. The fluorescence profile for the one-dimensional array of photodiodes corresponding to the electrophysiological recording sites is shown in Figure 4b. Again, the fluorescence profile does not show enough detail to allow a direct comparison with the results of the eCSD analysis: neither the synaptic activity nor the generation and propagation of action potentials is convincingly revealed. In contrast, the fluorescence-based iCSD profile (Fig. 4d) agrees quite well with the eCSD profile (Fig. 4c), both with respect to the excitatory postsynaptic potential (EPSP) pattern and to the propagation of population spike activity into the stratum oriens. However, spike activity in the stratum pyramidale is greatly reduced in the iCSD profile. This high-resolution iCSD profile, the result of a CSD transformation of the fluorescence map, will be explained in detail below. Before we actually describe the transformation itself, however, we list the set of assumptions made in its derivation.

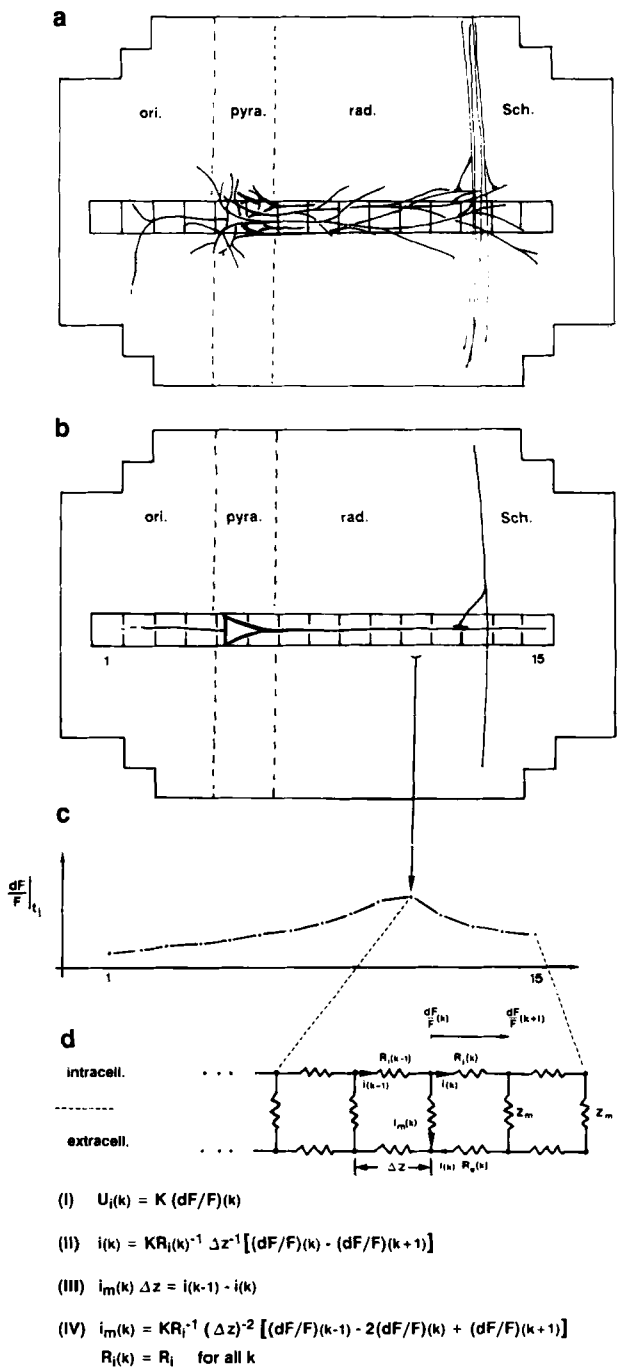

FIG. 5. CSD transformation of fluorescence maps, based on optical recordings using voltage-sensitive dyes, to iCSD profiles for the CA1 region of the rat hippocampal slice. A single photodiode column covers a number of CA1 pyramidal cells (a). Because of their orderly alignment and functional similarity, these cells can be merged into a single, hypothetical 'hyperneuron' (b). The photodiode column measures the spatial distribution of relative fluorescence change over neighbouring discrete compartments of this hyperneuron for successive time points t_i (c). The hyperneuron is modelled as a one-dimensional discrete cable equation. Each compartment k consists of an inner ohmic resistance $R_i(k)\Delta z$, an outer ohmic resistance $R_e(k)\Delta z$ and a membrane impedance Z_m (d). Notice that no assumption has to be made regarding the membrane impedance Z_m. The intracellular membrane potential in the kth compartment $U_i(k)$ is proportional to the relative fluorescence change dF/F in that compartment (d;I). For each moment t_i the current $i(k)$ flowing in the intracellular space between two compartments k and $k \times 1$ obeys Ohm's law. Hence, it follows from (d;I) that $i(k)$ is proportional to the difference between the relative fluorescence changes of these two compartments (d;II). The charge $i_m(k)\Delta z$ crossing the membrane from the intracellular space to the extracellular space is calculated by formula (d;III). Assuming a constant intracellular resistance $R_i(k) = R_i$ for all k, the iCSD $i_m(k)$ is proportional to the second-order spatial derivative of the relative fluorescence distribution (d;IV).

(1) The orientation of the linear photodiode array is parallel to the main orientation of the recorded CA1 cells.

(2) The distance between two photodiodes, as well as the area of tissue seen by each of them, is much smaller than the longitudinal extent of the activated cells.

(3) The activity measured by the selected photodiode column reflects the contributions from a whole group of similar cells. The number of cells that are covered completely by the photodiode column is considerably larger than the number of cells that are located on the border between two adjacent photodiode columns.

(4) The notion of 'cell' in this context stands not only for a special type of nerve cell but also for a functionally interconnected group of neurons [e.g. a pyramidal cell with recurrent inhibitory neuron(s)], under the condition that assumptions 2 and 3 hold.

(5) On the basis of assumptions 1–4 (see also Fig. 5a), we introduce the notion of the 'hyperneuron' (Fig. 5b): all cells within one photodiode column are regarded as a single, hypothetical hippocampal hyperneuron.

(6) We only consider 'fast' signals, and assume for the present purpose that the effect of glia depolarizations can be neglected.

(7) The hyperneuron can be modelled as a one-dimensional cable equation (Rall, 1962; Turner, 1984).

(8) The intracellular space can be approximated by a purely ohmic resistance.

(9) For any point in time, the distribution of relative fluorescence change dF/F over the photodiode column is proportional to the distribution of the intracellular membrane potential U_i along the hyperneuron (Fig. 5c):

$$U_i(k,t) = K\,(dF/F)(k,t) \tag{2}$$

with the proportionality constant K and compartment number k. For brevity we will omit reference to the time variable t from here on. It is to be understood, however, that each of the following equations holds for any point in time. The current $i(k)$ in the intracellular space between two adjacent compartments $k-1$ and k (measured by the corresponding photodiodes) can then be described by

$$i(k) = K\,R_{i-1}(k)\,\frac{(dF/F)(k) - (dF/F)(k+1)}{\Delta z} \qquad k \in [1,\ldots,m-1] \tag{3}$$

where m represents the total number of compartments and Δz is the width of a single compartment (i.e. the spatial sampling distance of the photodiode array). Hence, the current density $i_m(k)$ crossing the cell membrane between two compartments $k-1$ and k can be calculated as

$$i_m(k) = \frac{i(k-1) - i(k)}{\Delta z} \qquad k \in [2,\ldots,m] \tag{4}$$

From Equations 2–4, the current density $i_m(k)$ can be expressed in terms of the fluorescence signals by

$$i_m(k) = \frac{i(k-1) - i(k)}{\Delta z} \qquad k \in [2,\ldots,m-1]$$

$$= K\,\frac{(dF/F)(k-1) - (dF/F)(k)}{R_i(k-1)\Delta z^2} - K\,\frac{(dF/F)(k) - (dF/F)(k+1)}{R_i(k)\Delta z^2}$$

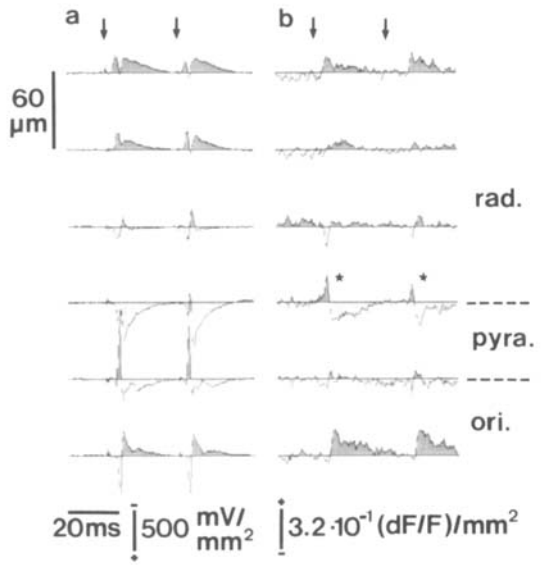

FIG. 6. eCSD (a) and iCSD (b) profiles in response to double-pulse stimulation of the Schaffer collaterals. Notice that the recording positions in this case were shifted over 30 μm with respect to the pyramidal cell layer boundaries as compared to Figure 4. Observe that this shift has a strong differential effect on the biphasic sink/source time course in the two profiles (★): in the eCSD the sink is reduced, whereas in the iCSD it is enhanced. Further details as in Figure 4.

$$= K \frac{(dF/F)(k-1) - 2\,(dF/F)(k) + (dF/F)(k+1)}{R_i(k-1)\Delta z^2} + \tag{5}$$

$$+ K \frac{R_i(k) - R_i(k-1)}{R_i(k)R_i(k-1)\Delta z} \frac{(dF/F)(k) - (dF/F)(k+1)}{\Delta z}$$

(10) If we further assume that to a first approximation the intracellular resistance is a constant in space, Equation 5 is reduced to only the first term:

$$i_m(k) = K \frac{(dF/F)(k-1) - 2\,(dF/F)(k) + (dF/F)(k+1)}{R_i z^2} \tag{6}$$

Keeping in mind that sinks/sources in the intracellular space are seen as sources/sinks from the extracellular space, we finally have to make a sign inversion to obtain the following proportionality relation:

$$I_m(z,t) \sim - \frac{(dF/F)(z - n\Delta z,t) - 2\,(dF/F)(z,t) + (dF/F)(z + n\Delta z,t)}{(n\Delta z)^2} \tag{7}$$

where z indicates the spatial dimension along the photodiode column and t denotes time. The integer n was set equal to 1. This then defines the CSD transformation which was applied to the fluorescence map in Figure 4b, the result of which is shown in Figure 4d. Observe that for the display of iCSD profiles, in order to account for the sign inversion in Equation 7 we inverted the plotting convention used for displaying eCSD profiles.

Summarizing, under assumptions 1–10, the one-dimensional iCSD profile for optical signals is proportional to minus the second-order spatial derivative of the distribution of relative fluorescence change. Notice the strong similarity between the iCSD transformation (Equation 7) and regular one-dimensional eCSD analysis (Equation 1): the role of the field potential U has simply been taken by the fluorescence signal dF/F.

Correspondence between iCSD and eCSD profiles

Returning now to the comparison of the two types of CSD profile in Figure 4c and d, we observe that the locations of the synaptic sink (indicated by the bracket) and its adjacent source in the more distal dendritic region (indicated by the star) coincide in the two pictures, while their time courses and amplitudes also agree quite well. Both the slower component, reflecting passive synaptic events, and the fast components, possibly due to 'hot spots' (arrowheads; Traub and Llinas, 1979; Plenz and Aertsen, 1993) are similar in both profiles. In contrast to this, population spike activity is strongly reduced in the iCSD profile, particularly in the stratum pyramidale. Nevertheless, the typical pattern of action potential propagation into the stratum oriens is clearly visible, especially in the facilitated response. These observations also apply to the other pairs of CSDs, not shown here: activity in the strata radiatum and oriens corresponds very well, whereas activity in the stratum pyramidale appears considerably smaller in the iCSD.

Since this mismatch between the two types of CSDs appears to affect predominantly the amplitude, rather than the time course of the signals, we investigated whether it can be described by a reduction in sensitivity for cell body activity in the iCSD. Such a reduction might be induced by a violation of our assumption 10, that the intracellular resistance along the dendrosomatic axis is constant. Therefore, we selected from each of the strata the traces with the most prominent features (maxima of EPSP, action potential and propagated action potential) and, after setting the activity in the stratum radiatum equal to 1, compared the relative amplitudes of these various features in the two CSDs. It turned out that in eCSD profiles the cell body activity is 4.0 ± 1.4 ($n = 17$) times as large as in iCSD profiles, while activity in the stratum oriens is approximately equal in the two CSDs (1.2 ± 0.4; $n = 16$). [Clearly, these factors are not dimensionless: a comparison of absolute eCSD and iCSD values in the stratum radiatum yields the physical dimensions of the scaling unit: $2.1 \pm 0.9 \times 10^3$ mV/(dF/F) ($n = 17$).]

This reduction in sensitivity in the cell body layer may make it difficult to distinguish the fast, biphasic waveform of the population spike in the iCSD. Moreover, this feature turns out to be critically dependent on the relative positioning of the photodiode array with respect to the pyramidal cell body layer. In particular, we often observed distinct signs of the population spike in traces from photodiodes overlying the transition between stratum pyramidale and stratum radiatum, as is demonstrated in Figure 6 (stars). We note that generally a similar critical dependence on recording position holds for the eCSD profiles, as illustrated by a closer comparison of Figures 4 and 6.

The question arises whether this general agreement between eCSD and iCSD also holds for stimulation of the alveus/stratum oriens region. The results of such an experiment are shown in Figure 7. Also in this case, results of the two approaches match quite well, with similar patterns of activity appearing in the two CSDs (Fig. 7c, d) in the stratum radiatum and stratum oriens. In the eCSD profile, multiple biphasic sink/source time courses in the stratum pyramidale (arrowheads in Fig. 7c) point to the generation of action potentials, presumably elicited antidromically and synaptically. These then invade the apical dendrites, as revealed by sinks propagating from the border of the stratum pyramidale into the stratum radiatum, and by delayed sources in the more distal parts of the dendritic region. Such antidromic invasion of action potentials into the stratum radiatum is also visible in the iCSD profile. However, in this case the multiple biphasic sink/source time courses, signifying the presence of population spike activity in the stratum pyramidale, are only indicated by small deflections (arrowheads in Fig. 7d). These deflections coincide with the sink-peaks of population spikes in the eCSD profile. Similar to the orthodromic stimulation experiment, the reduction in amplitude in the stratum pyramidale amounts to a factor of ~4.

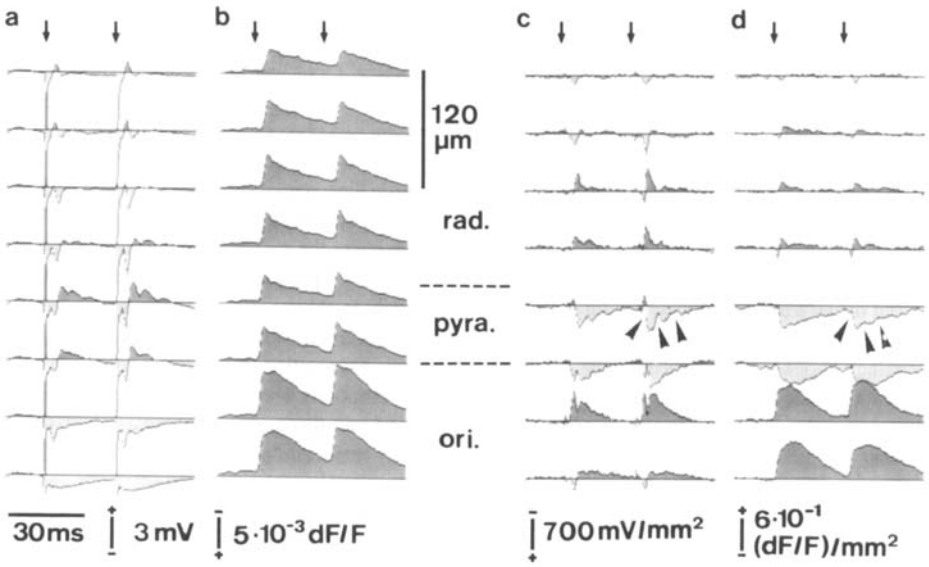

FIG. 7. Comparison of the eCSD profile and the iCSD profile in response to double-pulse stimulation of the alveus/stratum oriens region. (a) Field potential distribution. (b) Distribution of relative fluorescence change. (c) eCSD profile; (d) iCSD profile. Compare the amplitudes of the multiple biphasic sink/source time courses in both CSD profiles (arrowheads in c and d), reflecting the generation of population spikes in the stratum pyramidale. Further details as in Figure 4.

Finally, both CSD profiles exhibit a strong synaptic sink in the stratum oriens, indicating synaptic input to the basal dendrites and/or local interneurons.

Discussion

We compared two different experimental approaches to assess the spatio-temporal dynamics of neural activity: electrophysiological measurement of extracellular field potential distributions and optical recording of intracellular potential distributions by means of voltage-sensitive fluorescent dyes. These two measurements exhibit similar shortcomings in providing adequate spatial detail. Current source density analysis presents a common technique to enhance the spatial resolution of the field potential distributions. We propose a similar approach for the fluorescence maps: CSD analysis specifically designed for optical recordings. Before turning to this new CSD transformation and its experimental results, we will first discuss a number of methodological issues.

Dimensional approximation of the CSD pattern

To use the one-dimensional approximation (Equation 1) of a three-dimensional eCSD profile implies that contributions from the dimensions along the depth axis of the slice and along the CA1 region are disregarded. This could lead to differences between the calculated and the true CSD. We expect these differences to be small for a number of reasons, however. Nicholson and Freeman (1975) have shown that the one-dimensional approximation should be adequate under certain geometrical constraints; these are certainly fulfilled by the hippocampal CA1 region (Richardson *et al.*, 1987). Moreover, measurements along the axis perpendicular to the slice surface actually showed that at a particular depth (some 120 µm below the surface) contributions from that dimension to the eCSD can be neglected (Plenz and Aertsen, 1993). Possible effects on the amplitude, due to contributions from the dimension along the cell body layer (Novak and Wheeler, 1989) should be negligible in our case, because of the fine sampling grid. Finally, the additional assumption of a constant extracellular conductivity along the dendrosomatic axis is justified by the findings of Holsheimer (1987). To what extent such a one-dimensional approximation can also be expected to hold for iCSD profiles will be discussed in detail later.

Optical recording of 'intracellular population activity' maps

When optically recording the activity over an extended region of nervous tissue, it is practically impossible to determine the precise origin of the fluorescence signals collected by each single photodiode. Rather, one has to assume that each detector collects the contributions from a particular assortment of cell elements (dendritic branches, cell bodies) with varying surface-to-volume ratios. The absolute fluorescence F, measured by a single diode, is proportional to the amount of membrane-bound dye; this, in turn, is proportional to the available membrane surface (Grinvald *et al.*, 1988). The linearity of transduction from membrane potential to fluorescence signal causes the same proportionality to hold for the incremental fluorescence dF, evoked by changes in the membrane potentials as brought about by neural activity. This implies that in a homogeneous tissue area, i.e. with predominantly one type of cell element, the relative incremental fluorescence dF/F, being the ratio of the two, no longer depends on the particular surface-to-volume ratio prevailing in that area. Hence, for a photodiode recording from such an area, the relative change in fluorescence is directly proportional to the 'intracellular population membrane potential'. Moreover, the signals dF/F from different photodiodes, each one recording from a different but homogeneous population, e.g. one from dendrites only, another from cell bodies only, can be compared quantitatively, in spite of the different membrane compositions giving rise to these signals. For heterogeneous tissue areas, however, such linearity does not hold: in the fluorescence signal dF/F from a mixture of cell elements, those elements with high surface-to-volume ratio (such as dendrites and axons) will be over-represented as compared to those with low surface-to-volume ratio (cell bodies). Hence, the fluorescence signals recorded by an array of photodiodes from areas with varying mixtures of cell elements cannot be compared quantitatively. For the hippocampus with its orderly topography, we made the assumption of 'local homogeneity': each photodiode collects the activity from a more or less homogeneous tissue area; different diodes, however, may see different cell elements

dominating. Thus, we measure mainly apical dendritic activity in the stratum radiatum, cell body activity in the stratum pyramidale, and basal dendritic and axonal activity in the stratum oriens/alveus region. This assumption of local homogeneity, which allows the construction of the 'hyperneuron', is justified *a posteriori* by the good correspondence between eCSD and iCSD profiles. Hence, for the hippocampal slice preparation we expect a linear relation between the fluorescence signal dF/F and the intracellular potential distribution along the entire extent of the dendrosomatic axis.

This linearity across the entire slice is in clear contrast to the prevailing notion that optical signals from the stratum pyramidale are three to four times too small compared to signals from the stratum radiatum and, particularly, that this discrepancy should be explained by the different membrane surface-to-volume ratios in these strata (Grinvald *et al.*, 1988). On the basis of intracellular recordings in dendrites and in cell bodies (Wong *et al.*, 1979; Benardo *et al.*, 1982), as well as from theoretical considerations (Traub and Llinás, 1979), we expect depolarizations in both regions in response to orthodromic stimulation to be of the same order of magnitude. Indeed, for Schaffer collateral stimulation, we measured peak amplitudes of relative fluorescence change in the stratum pyramidale as high as 0.75 ± 0.15 ($n = 7$) times those in the stratum radiatum. Two effects would tend to decrease the relative amplitude in the cell body region. First, going 'downstream' from pulse stimulation of the Schaffer collaterals, via postsynaptic activity in the dendritic region to spike activity in the cell body region, the degree of synchrony and, hence, the amplitude of the population signal, is bound to decrease. Moreover, the population spike, being the ensemble average of *bi*phasic single cell action potentials, is more vulnerable to temporal dispersion than the synaptic potential, averaging over *mono*phasic postsynaptic potentials. Summarizing, we consider that the distribution of dF/F, measured along an appropriately chosen photodiode column, is truly representative of the intracellular voltage distribution at the population level.

In our preparations we could not discern any considerable slow component in the fluorescence signals. Since slow components in the relative fluorescence change are commonly attributed to glia depolarization (Lev-Ram and Grinvald, 1986; Konnerth *et al.*, 1987; Salzberg, 1989), we conclude that such glia depolarizations did not contribute significantly to our optical signals. However, we cannot rule out the possibility that part of the difference between eCSD and iCSD profiles should be attributed to possible differences in composition of the ensembles of signal sources, due to differential dye binding to neurons and to glia (Salzberg, 1989). Also, we could not distinguish any inhibitory components in the fluorescence signals, although these should in principle be expected (Schwartzkroin and Knowles, 1983; Buzsáki, 1984). One explanation might be that the inhibitory components were, in fact, present but that they were masked by the strong excitatory components of the fluorescence signal (Grinvald *et al.*, 1982b). Alternatively, it might be explained by an overall reduction of inhibition in the slice preparation; such a reduction might also account for the double-pulse facilitation in the extracellular field potential measurements (Figs 1, 4 and 6; Nathan *et al.*, 1990), which is in clear contrast to the situation *in vivo* and in organotypic cell cultures (Cornish and Wheal, 1989; Caeser *et al.*, 1990; Plenz and Aertsen, 1992).

CSD analysis of optical recording maps: iCSD profiles

In the construction of the hyperneuron and the subsequent calculation of the iCSD profile, a number of assumptions had to be made. For the CA1 region of the hippocampal slice, assumption 1 is easily fulfilled by properly orientating the photodiode array in parallel to the longitudinal axis of the orderly arranged pyramidal cells. The condition of sufficient spatial resolution of the photodiode matrix (assumption 2) is implicit in the reasoning on different cell compartments. A proper spacing of the optical recording grid should incorporate the anatomical dimensions of the neural elements involved. In addition, the minimal spatial distance between two photodiodes should be based upon a spatial Fourier analysis of the fluorescence distribution (Plenz and Aertsen, 1993). The drive towards high spatial resolution is counteracted, however, by assumption 3, which reflects a statistical argument. The aim of this assumption is to minimize the number of neurons that are not completely covered by a column of photodiodes. For the CA1 region we estimate that each photodiode column (diameter 60 μm) covers $\sim 50-100$ pyramidal cells, with a mean cell body diameter of $14-17$ μm (Richardson *et al.*, 1987). Hence, assumption 3 is clearly fulfilled.

Assumptions 4 and 5 concern the fact that the intracellular space is divided into disconnected compartments (the cells proper), in contrast to the extracellular space, which can be regarded as connected. Consequently, using Equation 7 to calculate the iCSD for two neighbouring intracellular compartments which in reality are disconnected would lead to deviations, due to the violation of border conditions (Rall, 1969). The assumption of a connected intracellular space can be justified, however, from a statistical point of view, at least for hippocampal pyramidal cells, because of their extensive arborization across the entire photodiode column. Similar reasoning holds for the approach of regarding a functionally interconnected group of neurons, for example a pyramidal cell together with its recurrent inhibitory interneuron(s), as a unitary 'cell'. From here on, assumption 5 is just a straightforward extension of assumptions $1-4$, arrived at by regarding the unitary modules, no longer depending on any specific anatomical features, as hypothetical hyperneurons. As discussed above, assumption 6 is clearly satisfied since significant contributions from glia–neuron interactions can be excluded in this preparation on the basis of the fast time course of the fluorescence signals.

Expanding on assumptions $1-6$, we modelled the hyperneuron as a one-dimensional, discrete cable equation (assumption 7). This approach, normally used to model single neurons (Rall, 1962; Turner, 1984), is applied here to describe the situation at the population level. The transmembrane current density is fully specified by the current distribution *along* the hyperneuron axis (Equation 4), which in turn is determined by the intracellular distribution of potential and impedance along that axis. Assumption 8, stating that this intracellular impedance can be considered as purely ohmic, is based on the ionic nature of the intracellular medium. The linear relationship between the fluorescence signal dF/F and the intracellular membrane potential (assumption 9) was discussed in the preceding section. The assumption of a constant *intra*cellular resistance along the dendrosomatic axis (assumption 10), which enables us to make the simplifying transition from Equation 5 to Equation 6, is the mirror image of a similar assumption regarding the *extra*cellular resistance, made in the derivation of the regular one-dimensional eCSD analysis (Equation 1). However, it clearly contradicts the observation that the intracellular resistance is a function of the diameter of the different cell compartments, and is regarded as being highest in the axonal branches, somewhat lower in the dendritic branches, and lowest in the cell body region. Indeed, a rough estimate on the basis of quantitative dimensions of pyramidal cell bodies and dendrites (Richardson, 1987; Schüz, personal communication) yields an intracellular resistance ratio between these different compartments in the range of $4-8$. Hence, the adoption of assumption 10 introduces a systematic error in the iCSD profiles, calculated on the basis of Equation 7: cell compartments with low intracellular resistance receive accordingly less weight than cell compartments with high intracellular resistance. This systematic error favours the activity in the dendritic and axonal

regions at the expense of the activity in the cell body region. The result is differential sensitivity of the iCSD in the different strata (Figs 4 and 6), which matches the estimate given above even quantitatively [scaling factor 4.0 ± 1.4 ($n = 17$)].

Summarizing, for the present experimental situation, the above considerations show that the list of assumptions 1–10 is indeed fulfilled. Hence, we conclude that the transformation described in Equation 7 provides an adequate prescription to estimate the true one-dimensional CSD distribution on the basis of optical recording signals.

Correspondence between iCSD and eCSD profiles

The comparison between fluorescence maps and iCSD profiles demonstrates that a transformation which involves taking the second spatial derivative provides a distinct improvement in spatial contrast. Clearly, this is not a surprising achievement, when we view the iCSD transformation as a mere image-processing technique. More interesting, however, is the direct and formal link we can make with the underlying physiological processes in terms of transmembrane current densities. In other words, the proposed transformation in Equation 7 is truly, both formally and substantially, a CSD transformation. This analogy between the two analytical approaches is based on the derivation of the actual iCSD transformation itself, together with the nature of the various assumptions made on the way. Thus, both measures of the eCSD and the iCSD profiles take fully analogous positions with respect to the presumed underlying CSD distribution: both involve additional convolutions reflecting the sample properties of the measurement probes used (microelectrodes versus photodiodes plus optical restrictions), and both involve inherent and fully analogous operational constraints (as discussed above). This analogy is emphasized by the surprisingly good correspondence we observed between iCSD profiles and classical eCSD profiles at the semiquantitative level. Many of the spatio-temporal features in the eCSD profiles are reproduced in the corresponding iCSD profiles in great detail, and vice versa. Yet a full quantitative correspondence between eCSD and iCSD profiles is nevertheless prohibited. First, the sample properties of the measurement probes are different in the two cases; this leads to quantitative differences in the two profiles, particularly for very localized events, such as action potentials and hot spots. Moreover, the operational constraints, expressed in the various assumptions, affect the outcome of the two analysis procedures in different ways, the most obvious example being that cell body activity in iCSD profiles is systematically diminished in comparison with eCSD profiles.

Summarizing, we conclude that iCSD profiles indeed furnish a more adequate basis for the interpretation of spatio-temporal patterns of nervous activity—mainly in terms of the underlying synaptic activity—than the amplitude–time distributions of the fluorescence maps do. From comparing many such profiles, however, we gained the distinct impression that, with the presently available voltage-sensitive dyes, CSD analysis at the same time presents an upper limit for the information which can be obtained from optical recordings of population activity in vertebrate tissue preparations. Hence, also in this respect, optical recording and extracellular measurements of field potential distributions are quite comparable.

The combination of optically recording the two-dimensional spatio-temporal distribution of nervous activity with subsequent enhancement of spatial contrast by calculating the iCSD profile is particularly useful for the investigation of the spreading of neural activity in anatomically ordered structures, such as the acute slice preparation (present study) and organotypic cultures (Plenz and Aertsen, 1992) of the hippocampus. To what extent this approach can also be used for the study of other nervous tissues, in particular those tissues with a less orderly anatomical organization, such as the neocortex, remains to be investigated. It is conceivable that in such tissues main directions can be defined on a more local scale, thereby constituting a 'vector field' of 'local main axes'.

Acknowledgements

We thank Dr Ulla Mitzdorf for helpful discussions in the early stage of this project, Dr Jürgen Bolz for his support in establishing the slice technique in our laboratory, and Volker Staiger for expert assistance in the experiments and in preparing the figures. The voltage-sensitive fluorescent dyes were kindly provided by Dr Amiram Grinvald. Partial funding for this project was received from the Bundesministerium für Forschung und Technologie.

Abbreviations

ACSF	artificial cerebrospinal fluid
ACSFKet	ACSF with ketamine added
CSD	current source density
dF/F	relative fluorescence change
eCSD	CSD based on extracellular field potential distribution
EPSP	excitatory postsynaptic potential
iCSD	CSD based on relative fluorescence maps

References

Andersen, P., Bliss, T. V. P. and Skrede, K. K. (1971) Unit analysis of hippocampal population spikes. *Exp. Brain Res.*, **13**, 208–221.

Benardo, L. S., Masukawa, L. M. and Prince, D. A. (1982) Electrophysiology of isolated hippocampal pyramidal dendrites. *J. Neurosci.*, **2**, 1614–1622.

Bonhoeffer, T. and Staiger, V. (1988) Optical recording with single cell resolution from monolayered slice cultures of rat hippocampus. *Neurosci. Lett.*, **92**, 259–264.

Buzsáki, G. (1984) Feed-forward inhibition in the hippocampal formation. *Prog. Neurosci.*, **22**, 131–153.

Caeser, M., Plenz, D. and Aertsen, A. M. H. J. (1990) Spatio-temporal spreading of electrical activity in rat hippocampus slices and cell cultures. In Elsner, N. and Roth, G. (eds), *Brain—Perception—Cognition.* Georg Thieme Verlag, Stuttgart.

Cohen, L. B. and Salzberg, B. M. (1978) Optical methods for monitoring neuron activity. *Annu. Rev. Neurosci.*, **1**, 171–182.

Cohen, L. B., Keynes, R. D. and Hille, B. (1968) Light scattering and birefringence during nerve activity. *Nature*, **218**, 438–441.

Creager, R., Dunwiddie, T. and Lynch, G. (1980) Paired-pulse and frequency facilitation in the CA1 region of the *in vitro* rat hippocampus. *J. Physiol. (Lond.)*, **299**, 409–424.

Grinvald, A., Hildesheim, R., Farber, I. C. and Anglister, L. (1982a) Improved fluorescent probes for the measurement of rapid changes in membrane potential. *Biophys. J.*, **39**, 301–308.

Grinvald, A., Manker, A. and Segal, M. (1982b) Visualization of the spread of electrical activity in rat hippocampal slices by voltage-sensitive optical probes. *J. Physiol. (Lond.)*, **333**, 269–291.

Grinvald, A., Frostig, R. D., Lieke, E. and Hildesheim, R. (1988) Optical imaging of neuronal activity. *Physiol. Rev.*, **68**, 1285–1366.

Holsheimer, J. (1987) Electrical conductivity of the hippocampal CA1 layers and application to current-source-density analysis. *Exp. Brain Res.*, **67**, 402–410.

Howland, B., Lettvin, J. Y., McCulloch, W. S., Pitts, W. and Wall, P. D. (1955) Reflex inhibition by dorsal root interaction. *J. Neurophysiol.*, **18**, 1–17.

Konnerth, A., Obaid, A. L. and Salzberg, B. M. (1987) Optical recordings of electrical activity from parallel fibres and other cell types in skate cerebellar slices. *J. Physiol. (Lond.)*, **393**, 681–702.

Lev-Ram, V. and Grinvald, A. (1986) Ca^{2+} and K^+ dependent communication between central nervous system myelinated axons and oligodendrites revealed by voltage-sensitive dyes. *Proc. Natl. Acad. Sci. USA*, **83**, 6651–6655.

Mitzdorf, U. (1985) Current source density method and application in cat cerebral cortex: Investigation of evoked potentials and EEG phenomena. *Physiol. Rev.*, **65**, 37–100.

Nathan, T., Jensen, M. S. and Lambert, J. D. C. (1990) $GABA_B$ receptors play a major role in paired-pulse facilitation in area CA1 of the rat hippocampus. *Brain Res.*, **531**, 55–65.

Nicholson, C. and Freeman, J. A. (1975) Theory of current source density analysis and determination of conductivity tensor for anuran cerebellum. *J. Neurophysiol.*, **38**, 356–368.

Novak, J. L. and Wheeler, B. C. (1989) Two-dimensional current source density

analysis of propagation delays for components of epileptiform bursts in rat hippocampus slices. *Brain Res.*, **497**, 223–230.

Orbach, H. S., Cohen, L. B. and Grinvald, A. (1985) Optical mapping of electrical activity in rat somatosensory and visual cortex. *J. Neurosci.*, **5**, 1886–1895.

Pitts, W. (1952) Investigations on synaptic transmission. In von Foerster, H. (ed.), *Cybernetics, Trans. 9th Conf.* Josiah Macypp, New York, pp. 159–162.

Plenz, D. and Aertsen, A. (1991) On the correspondence of intra- and extracellular space: convergence of classical field potential measurements and optical recording with voltage-sensitive dyes at the level of current source density analysis. In Penzlin, H. and Elsner, N. (eds), *Synapse—Transmission—Modulation*. Thieme Verlag, Stuttgart.

Plenz, D. and Aertsen, A. (1992) Current source density analysis of spatio-temporal fluorescence maps in organotypical slices cultures. In Aertsen, A. and Braitenberg, V. (eds), *Information Processing in the Cortex: Experiments and Theory*. Springer, Berlin, in press.

Plenz, D. and Aertsen, A. (1993) 'Hot spots' in the dendritic tree: local dendritic action potentials revealed by CSD analysis in the rat hippocampus slice. In preparation.

Rall, W. (1962) Electrophysiology of a dendritic neuron model. *Biophys. J.*, **2**, 145–167.

Rall, W. (1969) Time constants and electrotonic length of membrane cylinders and neurons. *Biophys. J.*, **9**, 1483–1508.

Richardson, L. T., Turner, R. W. and Miller, J. J. (1987) Action-potential discharge in hippocampal CA1 pyramidal neurons: current source-density analysis. *J. Neurophysiol.*, **58**, 981–996.

Ross, W. N., Salzberg, B. M., Cohen, L. B., Davila, H. V., Waggoner, A. S. and Chang, C. H. (1977) Changes in absorption, fluorescence, dichroism and birefringence in stained axons: optical measurement of membrane potential. *J. Membrane Biol.*, **33**, 141–183.

Salzberg, B. M. (1989) Optical recording of voltage changes in nerve terminals and in fine neuronal processes. *Annu. Rev. Physiol.*, **51**, 507–526.

Schwartzkroin, P. A. and Knowles, W. D. (1983) Local interaction in the hippocampus. *Trends Neurosci.*, **3**, 88–92.

Tasaki, I., Carnay, L. and Sandlin, R. (1969) Fluorescence changes during conduction in nerves stained with acridine orange. *Science*, **163**, 683–685.

Traub, R. D. and Llinas, R. (1979) Hippocampal pyramidal cells: Significance of dendritic ionic conductances for neuronal function and epileptogenesis. *J. Neurophysiol.*, **42**, 476–496.

Turner, D. A. (1984) Segmental cable evaluation of somatic transients in hippocampal neurons (CA1, CA3 and dentate). *Biophys. J.*, **46**, 73–84.

Waggoner, A. S. (1979) Dye indicators of membrane potential. *Annu. Rev. Biophys. Bioeng.*, **8**, 47–68.

Wong, K. S., Prince, D. A. and Basbaum, A. I. (1979) Intradendritic recordings from hippocampal neurons. *Proc. Natl. Acad. Sci. USA*, **2**, 986–990.